 CMES, vol.9, no.3, pp.221-233, 2005

3D Transient Heat Transfer by Conduction and Convection across a 2D Medium using a Boundary Element Model

N. Simões [1,2] and A. Tadeu [2]

Abstract: The use of the Boundary Element Method (BEM) to formulate the 3D transient heat transfer through cylindrical structures with irregular cross-sections, bounded by a homogeneous elastic medium, is described in this paper. In this formulation, both the conduction and the convection phenomena are modeled. This system can be subjected to heat emitted by either point or line sources located somewhere in the media. The solution is first obtained in the frequency domain for a wide range of frequencies and axial wavenumbers. Time domain responses are later calculated by means of (fast) inverse Fourier transforms into space-time. The appropriate fundamental solution (Green's functions) employed in this BEM model takes the convection phenomenon into account. The model is implemented and validated by comparing it with analytical solutions for a filled cylindrical circular ring core placed in an infinite medium and subjected to a heat line source.

keyword: Transient heat transfer, conduction, convection, Boundary Element Method, Green's functions.

1 Introduction

Most heat transfer problems involve heterogeneous elements and unsteady exchanges of energy between different media. Formulations for studying those systems should therefore contemplate transient heat phenomena. Several numerical approaches have been developed to study heat transfer. These include the Finite Elements [e.g. Bathe (1976)], the Finite Differences, the Boundary Elements Method [Brebbia *et al.* (1984), Pina and Fernandez (1984)] and Meshless techniques [Lin and Atluri (2000), Atluri and Shen (2002), Sladek *et al.* (2004)]. Of these techniques, the BEM only requires the discretization of the material boundaries, while it also takes into account the radiation conditions in the far field, which makes the description of the region quite compact. The Finite Elements and the Finite Differences Methods, however, need the full discretization of the domain being studied. The BEM is therefore an efficient method since fewer equations are needed. Furthermore, it is probably the method best suited to analyzing problems involving infinite or semi-infinite domains, since it automatically satisfies the far field conditions. Boundary Element models require the prior knowledge of Green's functions: the reference works by Carslaw and Jaeger (1959), Özisik (1993) and Beck (1992) contain compilations of certain Green's functions and their applicability.

Most of the known schemes devised to solve transient diffusion heat problems have either been formulated in the time domain ("time-marching" approach) or else they use Laplace transforms. The BEM has been employed in both techniques. In the "time-marching" approach, the BEM can be used to compute the solution directly in the time domain, step by step, at successive time increments. Chang *et al.* (1973) described the first time-domain direct boundary integral method to study planar transient heat conduction. Models involving time-dependent solutions were also proposed by: Shaw (1974), to deal with the heat diffusion in 3D bodies; Wrobel and Brebbia (1981), to study axisymmetric diffusion problems; Dargush and Banerjee (1991), to model planar, three-dimensional and axisymmetric analyses and Lesnic *et al.* (1995) to study unsteady diffusion equation in both one and two dimensions by a time marching BEM model, taking into account the treatment of singularities.

A disadvantage of the "time-marching" techniques is that their solutions may be unstable. An alternative is to apply a Laplace transform to move the solution from the time domain to a transformed variable. However, this process requires an inverse transform to find the solution in the time domain. Rizzo and Shippy (1970) used a Laplace transform associated with a boundary integral representation for transient heat conduction analysis. Since then, several authors have applied Laplace transforms to vari-

[1] nasimoes@dec.uc.pt

[2] Department of Civil Engineering, University of Coimbra, Pinhal de Marrocos, 3030-290 Coimbra, Portugal

ous diffusion problems, including Cheng *et al.* (1992), Zhu *et al.* (1994) and Sutradhar *et al.* (2002). The last author employed a Laplace transform BEM approach in a 3D transient heat conduction problem, considering that the thermal conductivity and the specific heat could change exponentially in one coordinate.

One drawback of using Laplace transforms is the loss of accuracy in the inversion process, which amplifies small truncation errors. Stehfest (1970) has proposed a more stable algorithm to overcome this problem. A time Fourier transform scheme has been suggested by the authors [Tadeu *et al.* (2004)] to deal with the time variable in the transient heat conduction equation. This approach allows the calculation to be made in the frequency domain.

In the work described here, the time Fourier Transform is again used to compute the transient heat transfer when cylindrical inclusions of infinite length are located inside a homogeneous elastic medium. However, the convection phenomenon is also considered in this formulation.

The rest of this paper is organized as follows: first, the fundamental equations of the three-dimensional heat diffusion problems are described; then, the main integrals required to solve the BEM are indicated, including the necessary Green's functions; next, the frequency heat responses through a cylindrical circular ring core are obtained using the BEM model and compared with analytical solutions; the BEM model is then used to simulate the heat propagation generated by a heat point source placed in the vicinity of an inclusion with an irregular cross-section, which encloses a circular cylinder.

2 Three-dimensional problem formulation

The transient heat transfer in a homogeneous, isotropic body, involving the conduction and convection phenomena, can be expressed by the diffusion equation below, when constant velocities, V_x, V_y and V_z, are assumed along the domain in the x, y and z directions respectively,

$$\nabla^2 T - \frac{1}{K}\left(V_x\frac{\partial T}{\partial x}+V_y\frac{\partial T}{\partial y}+V_z\frac{\partial T}{\partial z}\right)=\frac{1}{K}\frac{\partial T}{\partial t} \tag{1}$$

in which $\nabla^2=\left(\frac{\partial^2}{\partial x^2}+\frac{\partial^2}{\partial y^2}+\frac{\partial^2}{\partial z^2}\right)$, t is time, $T(t,\,x,\,y,\,z)$is temperature, $K=k/(\rho\,c)$is the thermal diffusivity, $k$is the thermal conductivity, ρ is the density and c is the specific heat. A Fourier transformation in the time domain applied to eq. (1) gives the equation below, expressed in the frequency domain

$$\left(\nabla^2-\frac{1}{K}\left(V_x\frac{\partial}{\partial x}+V_y\frac{\partial}{\partial y}+V_z\frac{\partial}{\partial z}\right)+\left(\sqrt{\frac{-\mathrm{i}\omega}{K}}\right)^2\right)\hat{T}(\omega,x,y,z)=0 \tag{2}$$

where $\mathrm{i}=\sqrt{-1}$ and ω is the frequency. Eq. (2) differs from the Helmholtz equation by the presence of a convective term. For a heat point source applied at $(0,0,\,0)$ in an unbounded medium, of the form $p(\omega,x,y,z,t)=\delta(x)\,\delta(y)\,\delta(z)\,e^{\mathrm{i}(\omega t)}$, where $\delta(y)$ and $\delta(z)$ are Dirac-delta functions, the fundamental solution of eq. (2) can be expressed as

$$\hat{T}_f(\omega,x,y,z)=\frac{e^{\frac{V_x x+V_y y+V_z z}{2K}}}{2k\sqrt{x^2+y^2+z^2}}e^{-\mathrm{i}\sqrt{-\frac{V_x^2+V_y^2+V_z^2}{4K^2}-\frac{\mathrm{i}\omega}{K}}\sqrt{x^2+y^2+z^2}} \tag{3}$$

When the geometry of the problem does not change along one direction (z) the full 3D problem can be expressed as a summation of simpler 2D solutions. This requires the application of a Fourier transformation along that direction, which can be expressed as a summation of 2D solutions with different spatial wavenumbers k_z[Tadeu & Kausel (2000)].

The application of a spatial Fourier transformation to $\frac{e^{-i\sqrt{-\frac{V_x^2+V_y^2+V_z^2}{4K^2}-\frac{\mathrm{i}\omega}{K}}\sqrt{x^2+y^2+z^2}}}{\sqrt{x^2+y^2+z^2}}$ along the z direction, leads to

$$\tilde{T}_f(\omega,x,y,k_z)=\frac{-\mathrm{i}\;e^{\frac{V_x x+V_y y+V_z z}{2K}}}{4k}H_0\left(\sqrt{-\frac{V_x^2+V_y^2+V_z^2}{4K^2}-\frac{\mathrm{i}\omega}{K}-(k_z)^2}\;r_0\right) \tag{4}$$

where H_0 are second-kind Hankel functions of the order 0, and $r_0=\sqrt{x^2+y^2}$.

This response is related to a spatially varying heat line source of the type $p(\omega,x,y,k_z,t)=\delta(x)\,\delta(y)\,e^{\mathrm{i}(\omega t-k_z z)}$ (see 1).

The full three-dimensional solution can be synthesized by applying an inverse Fourier transform along the k_z domain to the expression

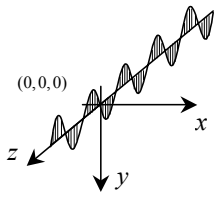

Figure 1 : Spatially harmonic varying line load

$\frac{-\mathrm{i}}{2} H_0\left(\sqrt{-\frac{V_x^2+V_y^2+V_z^2}{4K^2}-\frac{\mathrm{i}\omega}{K}-(k_z)^2}\, r_0\right)$. If we assume the existence of virtual sources, equally spaced sufficiently far apart, this inverse Fourier transformation can be formulated as a discrete summation, which enables the solution to be obtained by solving a limited number of two-dimensional problems,

$$\hat{T}(\omega,x,y,z) = \frac{2\pi}{L}\frac{e^{\frac{V_x x+V_y y+V_z z}{2K}}}{2k\sqrt{x^2+y^2+z^2}} \sum_{m=-M}^{M} H_0\left(\sqrt{-\frac{V_x^2+V_y^2+V_z^2}{4K^2}-\frac{\mathrm{i}\omega}{K}-(k_{zm})^2}\, r_0\right) e^{-\mathrm{i}k_{zm}z} \quad (5)$$

where k_{zm} is the axial wavenumber given by$k_{zm} = \frac{2\pi}{L_z}m$. The distance L_z must be large enough to prevent spatial contamination from the virtual sources [Bouchon & Aki (1977)]. An analogous approach has been used by Tadeu *et al* (2002) and Godinho *et al* (2001) to solve problems of wave propagation.

The fundamental solution of the differential equation obtained from eq. (2) after the application of a spatial Fourier transformation along the z direction is eq. (4) with $V_z = 0$.

$$\left(\tilde{\nabla}^2 - \frac{1}{K}\left(V_x\frac{\partial}{\partial x}+V_y\frac{\partial}{\partial y}\right)+\left(\sqrt{\frac{-\mathrm{i}\omega}{K}-(k_z)^2}\right)^2\right) \tilde{T}(\omega,x,y,k_z) = 0 \quad (6)$$

with $\tilde{\nabla}^2 = \left(\frac{\partial^2}{\partial x^2}+\frac{\partial^2}{\partial y^2}\right)$.

The frequency responses may need to be computed from 0.0Hz up to very high frequencies. However, since the heat responses decay very fast as the frequency increases, it allows us to limit the upper frequency where the solution is required. The use of complex frequencies leads to arguments for the Hankel function different from zero ($\omega_c = -i\eta$ for 0.0Hz), when the frequency is zero, which allows the calculation of the static response.

The heat responses in the spatial-temporal domain are then obtained by means of an inverse fast Fourier transform in k_z and in the frequency domain. In order to prevent the aliasing phenomena, complex frequencies with a small imaginary part of the form $\omega_c = \omega - \mathrm{i}\eta$ (with $\eta = 0.7\Delta\omega$, and $\Delta\omega$ being the frequency step) are used in the computation procedure. The constant η cannot be made arbitrarily large, since this leads to severe loss of numerical precision in the evaluation of the exponential windows [see Kausel and Roësset (1992)]. The time evolution of the heat source amplitude can be easily changed.

3 Boundary Element Method formulation

The fundamental BEM equations can be found in Wrobel (1981), where they are described in detail. The BEM can be used to solve eq. (6) for each value of k_z, corresponding to individual 2D problems.

The boundary integral equations for a homogeneous isotropic medium layer that is embedded in an infinite medium and contains a cylindrical body (bounded by a surface S), when this system is subjected to an incident heat field given by $\tilde{T}_{inc}$, are expressed as follows,

along the exterior domain

$$\begin{aligned}\overline{p}\,\tilde{T}^{(ext)}(x_0,y_0,k_z,\omega) &= \int_S q^{(ext)}(x,y,\eta_n,k_z,\omega)G^{(ext)}(x,y,x_0,y_0,k_z,\omega)\,ds \\ &- \int_S H^{(ext)}(x,y,\eta_n,x_0,y_0,k_z,\omega)\tilde{T}^{(ext)}(x,y,k_z,\omega)\,ds \\ &- \int_S G^{(ext)}(x,y,x_0,y_0,k_z,\omega)\tilde{T}^{(ext)}(x,y,k_z,\omega)V_n^{(ext)}\,ds \\ &+ \tilde{T}_{inc}(x_0,y_0,k_z,\omega) \end{aligned} \quad (7)$$

along the interior domain

$$\begin{aligned}\overline{p}\,\tilde{T}^{(int)}(x_0,y_0,k_z,\omega) &= \int_S q^{(int)}(x,y,\eta_n,k_z,\omega)G^{(int)}(x,y,x_0,y_0,k_z,\omega)\,ds \\ &- \int_S H^{(int)}(x,y,\eta_n,x_0,y_0,k_z,\omega)\tilde{T}^{(int)}(x,y,k_z,\omega)\,ds \\ &- \int_S G^{(int)}(x,y,x_0,y_0,k_z,\omega)\tilde{T}^{(int)}(x,y,k_z,\omega)V_n^{(int)}\,ds \end{aligned} \quad (8)$$

These boundary integral equations incorporate a term related to the convection phenomenon: $V_n = V_x n_x + V_y n_y$. In eqs. (7) and (8), the interior and exterior domains are identified by the superscripts *int* and *ext* respectively, ν_n is the unit outward normal along the boundary, G and H are respectively the fundamental solutions (Green's functions) for the temperature ($\tilde{T}$) and heat flux (q), at (x,y) due to a virtual point heat load applied at (x_0,y_0), $\overline{p}$ is a constant defined by the shape of the boundary, with a value of $1/2$ if $(x_0,y_0) \in S$ when the boundary is smooth. Note that this formulation assumes initial conditions of null temperatures and null heat fluxes throughout the domain. Other initial conditions would require the evaluation of the surface integrals.

If the boundary is discretized into N straight boundary elements, with one nodal point in the middle of each element, eqs. (7) and (8) take the form,

along the exterior domain

$$\sum_{l=1}^{N} q^{(ext)\,kl} G^{(ext)\,kl} - \sum_{l=1}^{N} \tilde{T}^{(ext)\,kl} H^{(ext)\,kl} - \sum_{l=1}^{N} G^{(ext)\,kl} \tilde{T}^{(ext)\,kl} V_n^{(ext)} + \tilde{T}^k_{inc_l} = c_{kl} \tilde{T}_l^{(ext)\,k} \tag{9}$$

along the interior domain

$$\sum_{l=1}^{N} q^{(int)\,kl} G^{(int)\,kl} - \sum_{l=1}^{N} \tilde{T}^{(int)\,kl} H^{(int)\,kl} - \sum_{l=1}^{N} G^{(int)\,kl} \tilde{T}^{(int)\,kl} V_n^{(int)} = c_{kl} \tilde{T}_l^{(int)\,k} \tag{10}$$

where $q_l^{(ext)\,kl}$ and $\tilde{T}_l^{(ext)\,kl}$ are the nodal heat fluxes and temperatures in the exterior domain, $q_l^{(int)\,kl}$ and $\tilde{T}_l^{(int)\,kl}$ are the nodal heat fluxes and temperatures in the interior domain,

$$H_l^{(ext)kl} = \int_{C_l} H^{(ext)}(\omega, x_l, y_l, \eta_l, x_k, y_k, k_z)\, dC_l$$

$$H_l^{(int)kl} = \int_{C_l} H^{(int)}(\omega, x_l, y_l, \eta_l, x_k, y_k, k_z)\, dC_l$$

$$G_l^{(ext)kl} = \int_{C_l} G^{(ext)}(\omega, x_l, y_l, x_k, y_k, k_z)\, dC_l$$

$$G_l^{(int)kl} = \int_{C_l} G^{(int)}(\omega, x_l, y_l, x_k, y_k, k_z)\, dC_l$$

where η_l is the unit outward normal for the l^{th} boundary segment C_l. In equations (9) and (10), $H^{(ext)}(\omega, x_l, y_l, \eta_l, x_k, y_k, k_z)$ and $G^{(ext)}(\omega, x_l, y_l, x_k, y_k, k_z)$ are respectively the Green's functions for the heat fluxes and temperature components in the exterior medium of the inclusion, while $H^{(int)}(\omega, x_l, y_l, \eta_l, x_k, y_k, k_z)$ and $G^{(int)}(\omega, x_l, y_l, x_k, y_k, k_z)$ are respectively the Green's functions for the heat fluxes and temperature components in the interior medium of the inclusion, at point(x_l, y_l), caused by a concentrated heat load acting at the source point (x_k, y_k). If the loaded element coincides with the element being integrated, the factor c_{kl} takes the value$1/2$.

The two-and-a-half dimensional Green's functions for temperature and heat fluxes in Cartesian co-ordinates are those for an unbounded medium,

$$G(x,y,x_0,y_0,k_z,\omega) = \frac{-\mathrm{i}}{4k} e^{\frac{V r_0}{2K}} H_0(k_{tr}\, r)$$

$$H(\omega, x_l, y_l, \eta_l, x_k, y_k, k_z) = \frac{-\mathrm{i}}{4} e^{\frac{V r_0}{2K}} \left[\frac{V}{2K} \left(\frac{\partial r_0}{\partial \eta_l} \right) H_0(k_{tr}\, r) - k_{tr} H_1(k_{tr}\, r) \left(\frac{\partial r}{\partial \eta_l} \right) \right] \tag{11}$$

where V is the radial convection velocity, $k_{tr} = \sqrt{\frac{-V^2}{4K^2} + \frac{-i\omega}{K} - (k_z)^2}$, $r = \sqrt{(x_l - x_k)^2 + (y_l - y_k)^2}$, $r_0 = \sqrt{x^2 + y^2}$ is the distance to the convection source position, and H_n are Hankel functions of the second kind and order n.

If the element to be integrated is not the loaded element, the integrations in equations (9) and (10) are evaluated using a Gaussian quadrature scheme, while for the loaded element, the existing singular integrands in the source terms of the Green's functions are calculated in closed form [Tadeu (1999)].

The final system of equations is assembled assuring the continuity of temperatures and heat fluxes along the boundary of the inclusion. The unknown nodal temperatures and heat fluxes are obtained by solving this system of equations, allowing the heat field along the domain to be defined.

The final integral equations are manipulated and combined so as to impose the continuity of temperatures and heat fluxes along the boundary of the inclusion, and a system of equations is assembled. The solution of this system of equations gives the nodal temperatures and heat fluxes, which allow the reflected heat field to be defined.

A numerical inverse fast Fourier transform in k_z and frequency domain is then used to compute the temperature field in the spatial-temporal domain.

4 Bem validation

The BEM algorithm was implemented and validated by applying it to a filled cylindrical circular ring core (see figure 2), subjected to a harmonic heat line source applied at point O (x_0, y_0), for which the solution is known in closed form and described in Appendix A. The continuity of normal heat fluxes and temperatures at both interfaces along the material interfaces ($a = 0.5\,\text{m}$ and $b = 1.0\,\text{m}$) are assumed. The thermal properties and the convection velocities allowed at each of the three media are listed in figure 1. The reflected heat responses were calculated in the frequency domain from 0 Hz to 64×10^{-7} Hz, with a frequency increment of $\Delta\omega = 1 \times 10^{-7}$ Hz and considering a single value of the parameter k_z equal to 0.4 rad / m. The simulated system is heated by a harmonic line source located in the inner medium of the circular ring core ($x = -0.3\,\text{m}, y = 0.0\,\text{m}$).

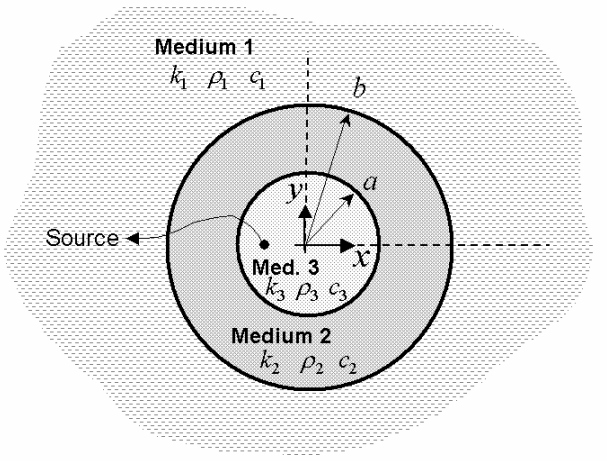

Figure 2 : Circular ring core geometry

Fig. 3 shows the real and imaginary parts of the responses at receivers placed in each medium: Rec. 1 ($x = 0.2\,\text{m}, y = 0.2\,\text{m}$), in medium 3; Rec. 2 ($x = 0.2\,\text{m}, y = 0.7\,\text{m}$), in medium 2; and Rec. 3 ($x = 0.2\,\text{m}, y = 1.2\,\text{m}$), in medium 1. The solid lines represent the analytical responses, while the marked points correspond to the BEM solution, computed using 100 constant boundary elements. The round and the triangle marks designate the real and imaginary parts of the responses, respectively. The results obtained by the two formulations are in very close agreement. Very good results were also obtained for heat sources and receivers placed at different positions.

5 Applications

The BEM formulation has been used to study the heat propagation in a system in which a hollow square (medium 2) is buried in an unbounded water medium (medium 1), and the square, 0.5 m length, contains a solid cylinder, 0.15 m of radius, which is filled with oil (medium 3), as illustrated in Figure 4. The inclusions have been modeled using a total of 500 straight boundary elements.

Two different cases have been considered ascribing different properties to the medium 2. The hollow square (containing the cylindrical ring core) (medium 2) is defined as being made of steel (Case 1) or concrete (Case 2), for which the thermal properties are listed in the figure 2. The thermal conductivity ($k_1 = 0.606\,\text{W.m}^{-1}.^{\circ}\text{C}^{-1}$), the density ($\rho_1 = 998.0\,\text{Kg.m}^{-3}$) and the specific heat ($c_1 = 4181.0\,\text{J.Kg}^{-1}.^{\circ}\text{C}^{-1}$) of the host medium (water) are kept constant in all the analyses and it is assumed that they do not vary with temperature. The thermal properties of the oil (medium 3) are assumed to remain constant with temperature variations, allowing $k_3 = 0.145\,\text{W.m}^{-1}.^{\circ}\text{C}^{-1}$, $\rho_3 = 887.1\ \text{Kg.m}^{-3}$ and $c_3 = 1888.5\,\text{J.Kg}^{-1}.^{\circ}\text{C}^{-1}$.

This system is subjected to a heat point source, placed in the host medium at ($x_0 = -0.15$ m, $y_0 = -0.1$ m, $z_0 = 0.0$ m), which starts emitting energy at $t \approx 0.76$ h. Its power is increased linearly from 0.0 W to 1000.0 W, reaching maximum power at $t \approx 3.46$ h. This peak is maintained for a period of $t \approx 2.72$ h. The power is then reduced linearly to 0.0 W, which occurs at $t \approx 8.89$ h. The heat field is computed for several grids of receivers in the frequency range of $\left[0.0,\ 128.0e^{-5}\text{Hz}\right]$, with a frequency increment of $0.5e^{-5}$ Hz, giving a time period of 55.56 h. The spatial intervals between virtual sources are given by the higher value of L, depending on the material's thermal properties, $L = (2\sqrt{k_i/(\rho_i\, c_i \Delta f)} + 2)$.

Next, two situations are presented: the modeling of both the conduction and convection phenomena, or the conduction phenomenon alone. The convection velocity (in the y direction) affecting the water medium may be $2.0 \times$

Table 1 : Material thermal properties

	Medium 1	**Medium 2**	**Medium 3**
Thermal conductivity $\left(\text{W.m}^{-1}.^{o}C^{-1}\right)$	$k_1 = 0.12$	$k_2 = 0.72$	$k_0 = 0.12$
Density $\left(\text{Kg.m}^{-3}\right)$	$\rho_1 = 1380.0$	$\rho_2 = 780.0$	$\rho_0 = 1380.0$
Specific heat $\left(\text{J.Kg}^{-1}.^{o}C^{-1}\right)$	$c_1 = 510.0$	$c_2 = 1860.0$	$c_0 = 510.0$
Convection velocity (m / s)	$V_1 = 1 \times 10^{-6}$	$V_2 = 2 \times 10^{-6}$	$V_3 = 1 \times 10^{-6}$

Table 2 : Thermal properties of medium 2

Medium 2	Thermal conductivity, k [W.m^{-1}.$^{o}C^{-1}$]	Specific heat, c [J.Kg^{-1}.$^{o}C^{-1}$]	Density, ρ [Kg.m^{-3}]
Steel	63.9	434.0	7832.0
Concrete	1.4	880.0	2300.0

10^{-6} m / s, while for the oil a velocity of 1×10^{-6} m / s is allowed.

Table 3 : Coordinates of receivers Rec. 1 to Rec. 5, placed at $z = 0.0$ m and $z = 0.5$ m

Receiver	x (m)	y (m)
Rec. 1	-0.1835	0.2563
Rec. 2	-0.1835	0.5601
Rec. 3	0.0063	0.2563
Rec. 4	0.1835	0.4335
Rec. 5	0.1835	0.5601

Figures 5 and 6 illustrate the temperature evolution recorded at receivers Rec. 1 to Rec. 5, located at $z = 0.0$ m and $z = 0.5$ m, respectively. The receivers are placed inside the inclusions and also in the host medium, as shown in Figure 4 and listed in Table 3.

Since null initial temperatures and heat fluxes are the initial conditions prescribed for the full domain, all the receivers exhibit null temperatures in the initial moments of the time responses. After the heat source has started emitting energy, the receiver closest to the heat source (Rec. 1), on plane $z = 0.0$ m, is the first to register a change of temperature. This same receiver also records a higher maximum temperature during the time domain under study than the rest of the receivers, for both cases. For Case 1, receiver Rec. 1 reaches almost 47.0 °C, while a maximum of 130.0 °C is registered when Case 2 is computed. At $z = 0.5$ m, when Case 1 is modeled, receiver Rec. 1 records a higher maximum temperature (23.2 °C) than the same receiver does in Case 2 (15.9 °C). For Case 1, the amplitude decreases 23.8 °C between the planes $z = 0.0$ m and $z = 0.5$ m, while the difference is 114.1 °C for the Case 2. We may conclude that in the presence of the hollow concrete inclusion, the energy does not propagate so easily in the z direction, as it does when the inclusion is made of steel. So, the amplitude differences between the two cases, found at $z = 0.0$ m, result from heat accumulation in the source plane ($z = 0.0$ m), when the inclusion medium presents a significantly lower thermal diffusivity.

At receiver Rec. 5, which is placed further away from the heat source, the temperature increase smoothly and its maximum is reached at later times (when the source power is no longer emitting energy), which means that the energy is still propagating to the zones with lower temperatures in order to achieve energy equilibrium.

The distances from the source to the receivers Rec. 3 and Rec. 4, located at $z = 0.0$ m, are 0.389 m and 0.629 m, respectively. Receiver Rec. 3 exhibits a far higher maximum temperature than Rec. 4 in Case 2 (concrete material). When steel is used, however, these receivers register similar maximum temperatures. We may also observe that although receivers Rec. 2 and Rec. 4, located at $z = 0.0$ m, are almost the same distance from the source, Rec. 4 registers a higher maximum temperature sooner than Rec. 2, in Case 1.

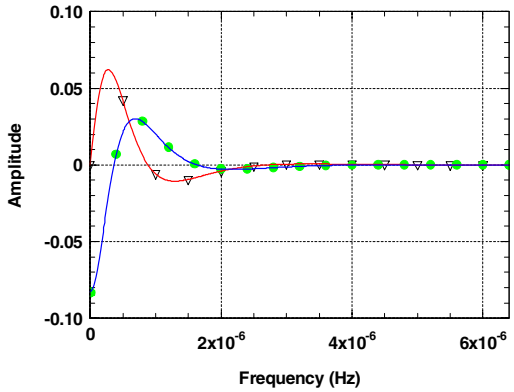

a)

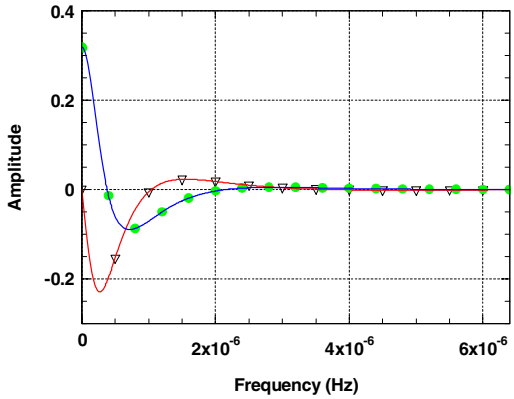

b)

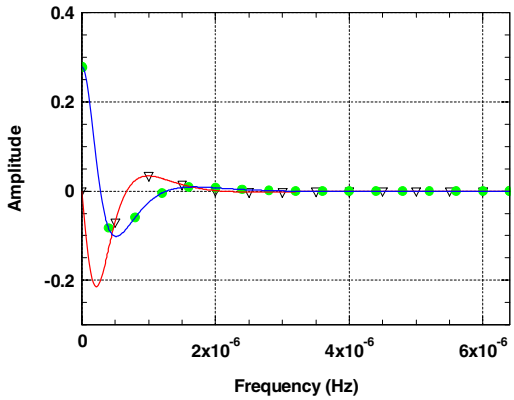

c)

Figure 3 : Real and imaginary parts of the heat responses when a heat source is placed in medium 3 ($x = -0.3\,\text{m}$, $y = 0.0\,\text{m}$): a) Receiver Rec. 1; b) Receiver Rec. 2; c) Receiver Rec. 3

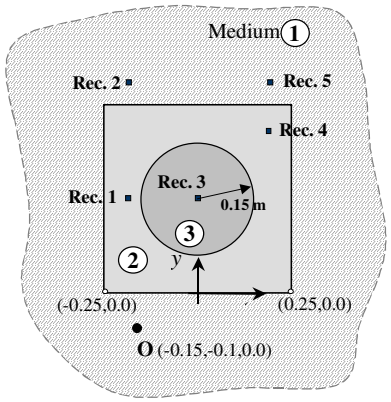

Figure 4 : Geometry of the problem and position of a set of receivers (Receivers Rec. 1 to Rec. 5) placed at $z = 0.0\,\text{m}$ and $z = 0.5\,\text{m}$

The factors involved in these dissimilar responses are related to the thermal diffusivity differences between the three media and also to the receivers' distance from the heat source. When no convection phenomenon is modeled, lower temperatures are recorded by all the receivers, as shown in figure 5. The presence, direction and amplitude of the convection velocity may have a considerable influence on the heat responses.

In figure 6 a set of snapshots, obtained at $t = 10$ h and $t = 20$ h, displays the temperature field for both cases, the hollow square steel and concrete structures. The results are presented using two-dimensional contour figures (transversal and longitudinal grid of receivers). These last illustrations are obtained from a transversal grid of receivers (80×80) placed at $z = 0.0\,\text{m}$ and from a longitudinal grid of receivers, distributed in the $x\,z$ plane, crossing the hollow inclusion at $y = 0.25$ m.

At $z = 0.0\,\text{m}$ and time $t = 10\,\text{h}$ it is interesting to note that round isothermals can be found within the oil domain for Case 1 (see figure 6a)), which means that the heat propagates faster around the steel structure than through the oil fluid. The temperature around the full circular fluid medium is similar and the heat propagation process for this fluid medium is from the boundary to the centre. However, when the hollow square is made of concrete it can be observed that the temperature distribution mostly depends on the distance between each point and the heat source, since the thermal diffusivity difference between media 2 and 3 is less than for the steel material. The receivers placed in the concrete medium, behind the cylindrical circular fluid medium (opposite to the source side),

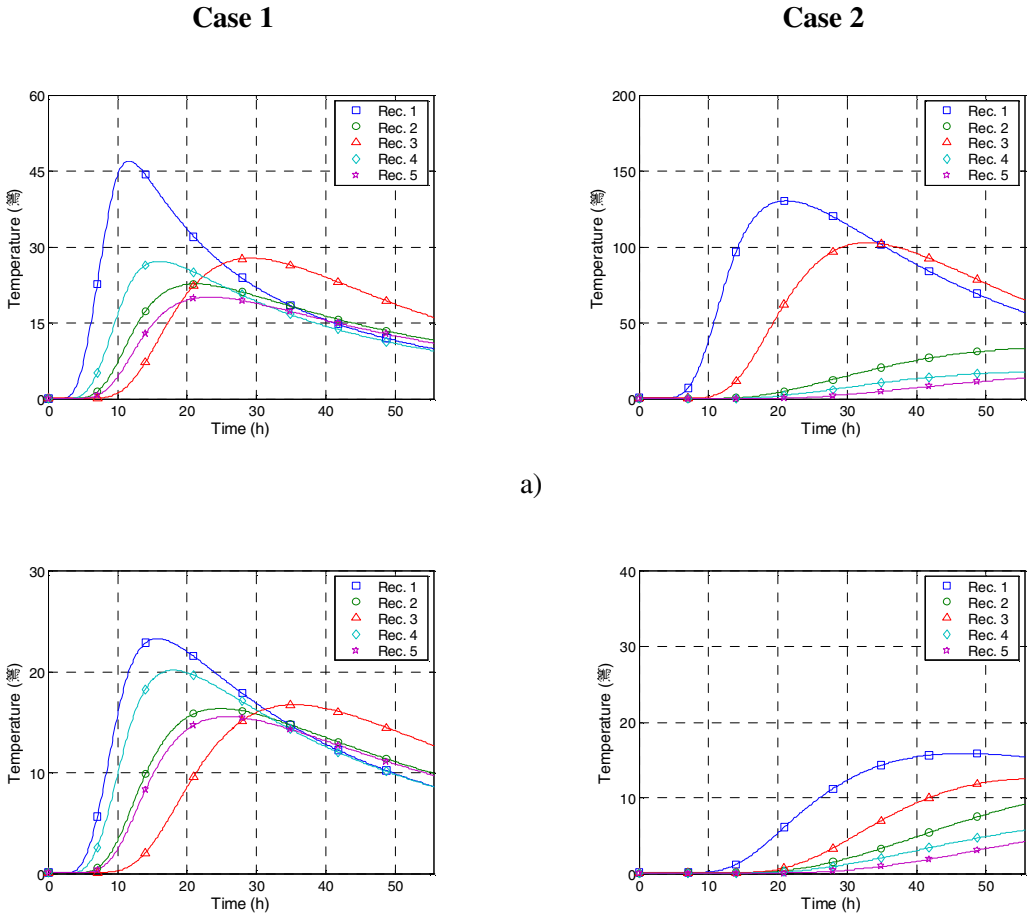

Figure 5 : Heat curves registered for Cases 1 and 2 when both conduction and convection phenomena are assumed: a) Receivers Rec. 1 to Rec. 5, placed at $z = 0.0$m; b) Receivers Rec. 1 to Rec. 5, placed at $z = 0.5$m

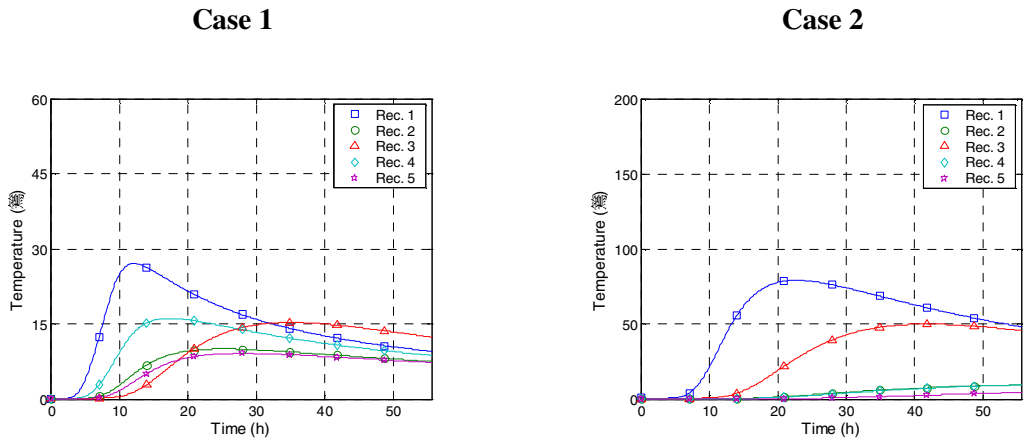

Figure 6 : Heat curves registered for Cases 1 and 2 when the conduction phenomenon is assumed alone: Receivers Rec. 1 to Rec. 5, placed at $z = 0.0$m

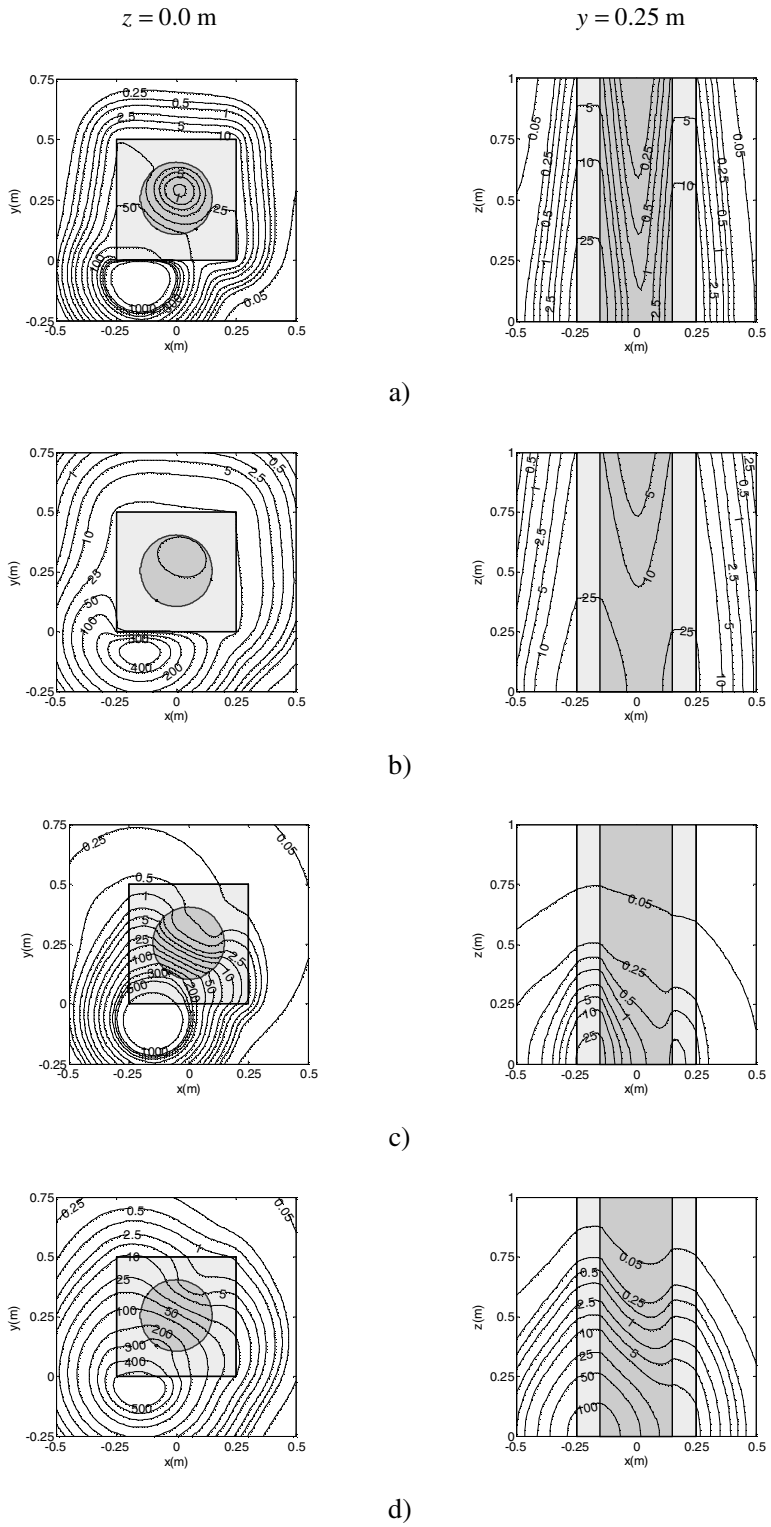

Figure 7 : Two-dimensional snapshots of the temperature fields (°C) when both conduction and convection phenomena are modelled: a) Case 1, at $t = 10h$; b) Case 1, at $t = 20h$; c) Case 2, at $t = 10h$; d) Case 2, at $t = 20h$

register lower temperatures along the transversal grid of receivers than the other regions that are the same distance from the source, which means that the heat flows through this inclusion more slowly. As time elapses, the temperature differences between the region behind the inclusion and in its vicinity decrease ($t = 20$ h in figure 6d)), confirming the equilibrium evolution. It is interesting to note also that the temperature rises in the zones a long away from the source, since the energy is still flowing away through the domain, while the temperature closer to the heat source decreases sharply.

The results computed at a grid of receivers distributed along the xz plane at $z = 0.025$ m are useful to better understand the heat diffusion process in the z direction. The receivers are spaced 0.025 m along the z direction: the grid is formed by 80×41 receivers.

Figures 7 c) and d) illustrate the high heat diffusivity [faster heat propagation] through the steel material: the presence of isothermals that are parallel with the x direction reflects this behaviour. The temperature distribution inside the oil reveals a long delay in the energy progress in the z direction. It is clear that the presence of the circular heterogeneity introduces an abrupt disruption of the heat propagation along the transversal domain.

6 Final Remarks

A BEM model has been implemented and used to compute three-dimensional transient heat transfer along a square hollow inclusion of infinite length, itself containing an inclusion filled with oil, located inside a homogeneous elastic medium and heated by a spherical heat load placed inside the host medium. The phenomena studied here include heat conduction and convection. The incorporation of convection diffusion changes the heat responses in keeping with the amplitude and velocities assumed for each material.

A Fourier transform applied in the time domain is the technique used to deal with the time variable of the diffusion equation. Notice that, if the geometry does not vary along one direction, the solution becomes simpler, since the full 3D problem can be computed as a summation of 2D solutions with different spatial k_z wavenumbers. The application of an inverse Fourier transform along the k_z domain can be expressed as a discrete summation if a sequence of sources, equally-spaced, is considered. A numerical inverse fast Fourier transform in k_z and in the frequency domain is then used to compute the temperature field in the spatial-temporal domain.

References

Bathe, K. J. (1976): Numerical Methods in Finite Element Analysis. New Jersey: Prentice-Hall.

Brebbia, C. A.; Telles, J. C.; Wrobel, L. C. (1984): Boundary Elements Techniques: Theory and Applications in Engineering. Berlin-New York: Springer-Verlag.

Pina, M. L. G.; Fernandez, J. L. M. (1984): Applications in heat conduction by BEM. In: C. A Brebbia (ed.) *Topics in Boundary Element Research*, Springer, Berlin.

Lin, H.; Atluri, S.N. (2000): Meshless Local Petrov-Galerkin (MLPG) Method for Convection-Diffusion Problems. *CMES: Computer Modeling in Engineering & Sciences*, vol. 1(2), pp. 45-60.

Atluri, S. N.; Shen, S. (2002): The Meshless Local Petrov-Galerkin (MLPG) Method: A Simple \& Less-costly Alternative to the Finite Element and Boundary Element Methods. *CMES: Computer Modeling in Engineering & Sciences*, vol. 3(1), pp. 11-52.

Sladek, J.; Sladek, V., Atluri, S.N. (2004): Meshless Local Petrov-Galerkin Method for Heat Conduction Problem in an Anisotropic Medium. *CMES: Computer Modeling in Engineering & Sciences*, vol. 6(3), pp. 309-318.

Carslaw, H. S.; Jaeger, J. C. (1959): Conduction of heat in solids. Second edition, New York: Oxford University Press.

Özisik, M. N. (1993): Heat Conduction. Second edition, New York: John Wiley & Sons.

Beck, J. V.; Cole, K. D.; Haji-Sheikh, A.; Litkouhi, B. (1992): Heat Conduction using Green's Functions. Washington, DC: Hemisphere Publishing Corporation.

Chang, Y. P.; Kang, C. S.; Chen D. J. (1973): The Use of Fundamental Green Functions for Solution of Problems of Heat Conduction in Anisotropic Media. *Int. J. Heat and Mass Transfer*, 16, pp. 1905-1918.

Shaw R. P. (1974): An Integral Equation Approach to Diffusion. *Int. J. Heat and Mass Transfer*, vol. 17, pp. 693-699.

Wrobel, L. C.; Brebbia, C. A. (1981): A Formulation of the Boundary Element Method for Axisymmetric Transient Heat Conduction. *Int. J. Heat and Mass Transfer*, Vol. 24, pp. 843-850.

Dargush, G. F.; Banerjee P. K. (1991): Application of the Boundary Element Method to Transient Heat Conduction. *Int. J. Numerical Methods in Engineering*, vol. 31, 1231-1247.

Lesnic, D.; Elliot L.; Ingham DB. (1995): Treatment of Singularities in Time-dependent Problems using the Boundary Element Method. *Engineering Analysis with Boundary Elements-EABE*, vol. 16, pp. 65-70.

Rizzo, F. J.; Shippy, D. J. (1970): A Method of Solution for Certain Problems of Transient Heat Conduction. *AIAA Journal*, Vol. 8, pp. 2004-2009.

Cheng, A.; Abousleiman, Y.; Badmus, T. (1992): A Laplace Transform BEM for Axisymmetric Diffusion Utilizing Pre-tabulated Green's Function. *Engineering Analysis with Boundary Elements-EABE*, vol. 9, pp. 39-46.

Zhu, S.P.; Satravaha, P.; Lu, X. (1994): Solving the Linear Diffusion Equations with the Dual Reciprocity Methods in Laplace Space. *Engineering Analysis with Boundary Elements-EABE*, vol. 13, pp. 1-10.

Sutradhar, A.; Paulino, G. H.; Gray, L. J. (2002): Transient Heat Conduction in Homogeneous and Non-Homogeneous Materials by the Laplace Transform Galerkin Boundary Element Method. *Engineering Analysis with Boundary Elements-EABE*, vol. 26 (2), pp. 119-132.

Stehfest, H. (1970): Algorithm 368: Numerical Inversion of Laplace Transform. *Communications of the Assoc. Comp. Machinery*, vol. 13(1), pp. 47-49.

Tadeu, A.; António, J.; Simões, N. (2004): 2.5D Green's Functions in the Frequency Domain for Heat Conduction Problems in Unbounded, Half-space, Slab and Layered Media. Computer *Modeling in Engineering & Sciences - CMES*, vol. 6(1), pp. 43-58.

Tadeu, A; Kausel E. (2000): Green's Functions for Two-and-a-half Dimensional Elastodynamic Problems. *J. Engng. Mechanics – ASCE*, vol. 126(10), pp. 1093-1097.

Bouchon, M.; Aki, K. (1977): Discrete Wave-number Representation of Seismic-source Wave Field. *Bulletin of the Seismological Society of America*, vol. 67, pp. 259-277.

Tadeu, A.; Godinho, L.; Santos P. (2002): Wave Motion Between Two Fluid Filled Boreholes in an Elastic Medium, *Engineering Analysis with Boundary Elements-EABE*, vol. 26(2), pp. 101-117.

Godinho, L.; António, J.; Tadeu, A. (2001): 3D Sound Scattering by Rigid Barriers in the Vicinity of Tall Buildings. Journal of Applied Acoustics, vol. 62(11), pp. 1229-1248.

Kausel, E.; Roësset, J. M. (1992): Frequency Domain Analysis of Undamped Systems. *Journal of Engineering Mechanics, ASCE*, vol. 118(4), pp. 721-734.

Tadeu, A.; Santos, P.; Kausel, E. (1999): Closed-form Integration of Singular Terms for Constant, Linear and Quadratic Boundary Elements -Part I: SH Wave Propagation. *Engineering Analysis with Boundary Elements-EABE*, vol. 23(8), pp. 671-681.

Tadeu, A.; Santos, P.; Kausel, E. (1999): Closed-form Integration of Singular Terms for Constant, Linear and Quadratic Boundary Elements - Part II: SV-P Wave Propagation, *Engineering Analysis with Boundary Elements-EABE,* vol. 23(9), pp. 757-768.

Watson, G. N. (1980): A Treatise on the Theory of Bessel Functions, second edition, Cambridge University Press.

Appendix A: Analytical Solution of the 3D Transient Heat Transfer through a Cylindrical Circular Ring Core

Consider a ring defined by the internal and external radii, a and b respectively, bounded by an exterior and interior medium, as illustrated in figure 8. This ring is heated by a harmonic source with radial convection, placed in the exterior solid medium (with a thermal conductivity k_1, a density ρ_1, a specific heat c_1 and a convection velocity V_1). The heat generated by this source propagates and hits the outer surface of the ring. After striking the outer surface of the cylindrical ring, part of the incident energy is reflected back into the exterior solid medium, and the remaining energy is transmitted into the ring material (with a thermal conductivity k_2, a density ρ_2, a specific heat c_2 and a convection velocity V_2), in the form of propagating energy. This energy continues to propagate and until it strikes the inner surface of the ring. There, a similar phenomenon may occur, with part of the energy being transmitted to the inner medium (with a thermal conductivity k_3, a density ρ_3, a specific heat c_3 and a convection velocity V_3) and the rest being reflected back to the ring medium. This process will be repeated until all the energy is dissipated.

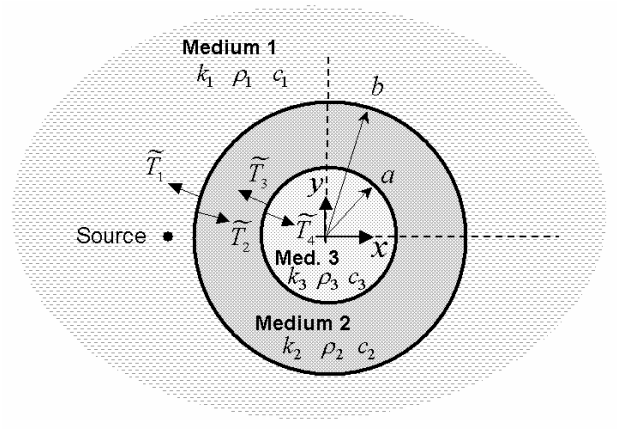

Figure 8 : Circular ring geometry and representation of the surface terms

Incident heat field (or free-field)

The three-dimensional incident field for a point pressure source placed at (x_0,0,0), can be expressed as

$$\hat{T}_{inc}(\omega,r,r',z)=\frac{Ae^{\frac{V_1 r}{2K_1}}}{2k_1}\frac{e^{-\mathrm{i}\sqrt{-\frac{V_1^2}{4K_1^2}-\frac{\mathrm{i}\omega}{K_1}}\sqrt{r'^2+z^2}}}{\sqrt{r'^2+z^2}}$$
$$\text{with } r'=\sqrt{(x-x_0)^2+y^2} \tag{12}$$

where the subscript *inc* denotes the incident field, A is the heat amplitude, $K_1=\frac{k_1}{\rho_1 c_1}$ and r' defines the distance between the source and the receiver. When a Fourier transformation is applied along the z direction, the incident field can be expressed as a summation of 2D sources, with different spatial wavenumbers,

$$\hat{T}_{inc}(\omega,r,r')=\frac{2\pi}{L}\sum_{m=-M}^{M}\tilde{T}_{inc}(\omega,r,r',k_{zm})\,e^{-\mathrm{i}k_{zm}z} \tag{13}$$

with $\tilde{T}_{inc}(\omega,r,k_{zm})=\frac{-\mathrm{i}A}{4k_1}e^{\frac{V_1 r}{2K_1}}H_0(k_{\alpha 1}r')$ and $k_{\alpha_1}=\sqrt{\frac{-V_1^2}{4K_1^2}+\frac{-\mathrm{i}\omega}{K_1}-(k_{zm})^2}$.

Eq. (13) expresses the incident field as heat terms centred at the source point (x_0, 0, 0), and not at the axis of the cylindrical inclusion, and this constitutes a difficulty. In order to overcome this problem, the incident heat field can be expressed as heat terms centred at the origin. This is achieved by applying Graf's addition theorem [Watson (1980)], which results in the expressions below (in cylindrical coordinates):

$$\tilde{T}_{inc}(\omega,r,\theta,k_{zm})=-\frac{\mathrm{i}A}{4k_1}e^{\frac{V_1 r}{2K_1}}\sum_{n=0}^{\infty}(-1)^n\varepsilon_n J_n(k_{\alpha_1}r_0)H_n(k_{\alpha_1}r)\cos(n\theta)$$
$$\text{when } r>r_0$$

$$\tilde{T}_{inc}(\omega,r,\theta,k_{zm})=-\frac{\mathrm{i}A}{4k_1}e^{\frac{V_1 r}{2K_1}}\sum_{n=0}^{\infty}(-1)^n\varepsilon_n H_n(k_{\alpha_1}r_0)J_n(k_{\alpha_1}r)\cos(n\theta),$$
$$\text{when } r<r_0, \tag{14}$$

in which r_0 is the distance from the source to the axis of the inclusion, $J_n(\dots)$ are Bessel functions of order n, and $\varepsilon_n=\begin{cases}1 & if \quad n=0\\ 2 & if \quad n\neq 0\end{cases}$.

The scattered heat field in the outer medium

The heat generated in the exterior medium depends on heat coming from the external surface of the cylindrical ring, which propagates away from it. The outgoing heat can be defined using the following equation,

$$\tilde{T}_1(\omega,r,\theta,k_{zm})=e^{\frac{V_1 r}{2K_1}}\sum_{n=0}^{\infty}A_n H_n(k_{\alpha_1}r)\cos(n\theta) \tag{15}$$

where A_n are unknown amplitudes.

The heat field in the ring

Two distinct groups of heat fields exist inside the ring, corresponding to the heat generated at the external surface and travelling inwards, and to the heat generated at the internal surface of the pipe, which travels outwards. For the terms generated at the external boundary, the corresponding standing heat field is given by

$$\tilde{T}_2(\omega,r,\theta,k_{zm})=e^{\frac{V_2 r}{2K_2}}\sum_{n=0}^{\infty}B_n J_n(k_{\alpha_2}r)\cos(n\theta) \tag{16}$$

where B_n are unknown amplitudes.

For the heat generated at the internal boundary, there is a corresponding diverging heat field, which can be defined by,

$$\tilde{T}_3(\omega,r,\theta,k_{zm})=e^{\frac{V_3 r}{2K_3}}\sum_{n=0}^{\infty}C_n H_n(k_{\alpha_3}r)\cos(n\theta) \tag{17}$$

where $k_{\alpha_3}=\sqrt{\frac{-V_3^2}{4K_3^2}+\frac{-\mathrm{i}\omega}{K_3}-(k_{zm})^2}$ and C_n are unknown amplitudes.

The heat field in the inner medium

In the inner medium (medium 3), the heat field depends only on heat coming from the internal surface of the cylindrical ring core, and thus only inward-propagating heat is generated. The corresponding heat field is given by:

$$\tilde{T}_4(\omega, r, \theta, k_{zm}) = e^{\frac{V_3 r}{2K_3}} \sum_{n=0}^{\infty} D_n J_n(k_{\alpha_3} r)\cos(n\theta) \tag{18}$$

where D_n are unknown amplitudes.

The unknown coefficients A_n, B_n, C_n and D_n are determined by imposing the required boundary conditions. For the case described here, the boundary conditions are the continuity of temperatures and normal heat fluxes on the two interfaces. The four equations defined give rise to a system of four equations with four unknowns, which yields the unknown coefficients.

$$\tilde{T}_{inc}(\omega, b, \theta, k_{zm}) + \tilde{T}_1(\omega, b, \theta, k_{zm}) = \tilde{T}_2(\omega, b, \theta, k_{zm}) \quad \text{at } r = b$$

$$k_1 \frac{\partial\left[\tilde{T}_{inc}(\omega, b, \theta, k_{zm})\right]}{\partial r} + k_1 \frac{\partial\left[\tilde{T}_1(\omega, b, \theta, k_{zm})\right]}{\partial r} = k_2 \frac{\partial\left[\tilde{T}_2(\omega, b, \theta, k_{zm})\right]}{\partial r} \quad \text{at } r = b$$

$$\tilde{T}_2(\omega, a, \theta, k_{zm}) + \tilde{T}_3(\omega, a, \theta, k_{zm}) = \tilde{T}_4(\omega, a, \theta, k_{zm}) \quad \text{at } r = a$$

$$k_2 \frac{\partial\left[\tilde{T}_2(\omega, a, \theta, k_{zm})\right]}{\partial r} + k_2 \frac{\partial\left[\tilde{T}_3(\omega, a, \theta, k_{zm})\right]}{\partial r} = k_3 \frac{\partial\left[\tilde{T}_4(\omega, a, \theta, k_{zm})\right]}{\partial r} \quad \text{at } r = a \tag{19}$$

Combining eqs. (A.3) and eqs. from (15) to (A.8) one obtains a system of equations which is then used to find the unknown coefficients (A_n, B_n, C_n, D_n):

$$\begin{bmatrix} a_{11} & a_{12} & a_{13} & a_{14} \\ a_{21} & a_{22} & a_{23} & a_{24} \\ a_{31} & a_{32} & a_{33} & a_{34} \\ a_{41} & a_{42} & a_{43} & a_{44} \end{bmatrix} \begin{bmatrix} A_n \\ B_n \\ C_n \\ D_n \end{bmatrix} = (-1)^n \varepsilon_n \begin{bmatrix} b_1 \\ b_2 \\ b_3 \\ b_4 \end{bmatrix} \tag{20}$$

with

$$a_{11} = e^{\frac{V_1 b}{2K_1}} H_n(k_{\alpha_1} b);$$

$$a_{12} = -e^{\frac{V_2 b}{2K_2}} J_n(k_{\alpha_2} b);$$

$$a_{13} = -e^{\frac{V_2 b}{2K_2}} H_n(k_{\alpha_2} b);$$

$$a_{14} = 0;$$

$$a_{21} = 0;$$

$$a_{22} = e^{\frac{V_2 a}{2K_2}} J_n(k_{\alpha_2} a);$$

$$a_{23} = e^{\frac{V_2 a}{2K_2}} H_n(k_{\alpha_2} a);$$

$$a_{24} = e^{\frac{V_3 a}{2K_3}} J_n(k_{\alpha_3} a);$$

$$a_{31} = k_1 \left\{ \begin{array}{c} \frac{V_1 b}{2K_1} H_n(k_{\alpha_1} b) + \\ [n H_n(k_{\alpha_1} b) - (k_{\alpha_1} b) H_{n+1}(k_{\alpha_1} b)] \end{array} \right\} e^{\frac{V_1 b}{2K_1}};$$

$$a_{32} = -k_2 \left\{ \begin{array}{c} \frac{V_2 b}{2K_2} J_n(k_{\alpha_2} b) + \\ [n J_n(k_{\alpha_2} b) - (k_{\alpha_2} b) J_{n+1}(k_{\alpha_2} b)] \end{array} \right\} e^{\frac{V_2 b}{2K_2}};$$

$$a_{33} = -k_2 \left\{ \begin{array}{c} \frac{V_2 b}{2K_2} H_n(k_{\alpha_2} b) + \\ [n H_n(k_{\alpha_2} a) - (k_{\alpha_2} a) H_{n+1}(k_{\alpha_2} b)] \end{array} \right\} e^{\frac{V_2 b}{2K_2}};$$

$$a_{34} = 0;$$

$$a_{41} = 0;$$

$$a_{42} = k_2 \left\{ \begin{array}{c} \frac{V_2 a}{2K_2} J_n(k_{\alpha_2} a) + \\ [n J_n(k_{\alpha_2} a) - (k_{\alpha_2} a) J_{n+1}(k_{\alpha_2} a)] \end{array} \right\} e^{\frac{V_2 a}{2K_2}};$$

$$a_{43} = k_2 \left\{ \begin{array}{c} \frac{V_2 a}{2K_2} H_n(k_{\alpha_2} a) + \\ [n H_n(k_{\alpha_2} a) - (k_{\alpha_2} a) H_{n+1}(k_{\alpha_2} a)] \end{array} \right\} e^{\frac{V_2 a}{2K_2}};$$

$$a_{44} = -k_3 \left\{ \begin{array}{c} \frac{V_3 a}{2K_3} H_n(k_{\alpha_3} a) + \\ [n J_n(k_{\alpha_3} a) - (k_{\alpha_3} a) J_{n+1}(k_{\alpha_3} a)] \end{array} \right\} e^{\frac{V_3 a}{2K_3}};$$

$$b_1 = \frac{\mathrm{i}A}{4k_1} e^{\frac{V_1 b}{2K_1}} H_n(k_{\alpha_1} r_0) J_n(k_{\alpha_1} b);$$

$$b_2 = 0;$$

$$b_3 = \frac{\mathrm{i}A}{4} e^{\frac{V_1 b}{2K_1}} H_n(k_{\alpha_1} r_0) \left\{ \begin{array}{c} \frac{V_1 b}{2K_1} J_n(k_{\alpha_1} b) + \\ \left[\begin{array}{c} n J_n(k_{\alpha_1} b) \\ -(k_{\alpha_1} b) J_{n+1}(k_{\alpha_1} b) \end{array} \right] \end{array} \right\};$$

$$b_4 = 0.$$

Notice that when the position of the heat source is changed, the terms a_{ij} of the matrix remain the same, while the independent terms b_i are different. However, as the equations can be easily manipulated to consider another position for the source, they are not included here.